Go4Hybrid

Deliverable D2.2-21

Preliminary report on performance of non-zonal methods

Date of issue

11 September 2015

Name of Author(s) : **J.C. Kok (NLR), M. Fuchs (CFDB), M. Strelets (NTS), and S.-H. Peng (FOI)**

Organisation :

NLR
Flight Physics and Loads Department
Anthony Fokkerweg 2
1059 CM Amsterdam, the Netherlands
Telephone no.: +31 88 5113020
E-Mail: johan.kok@nlr.nl

Approved by:

Author	Reviewer	Managing department
(11/9/2015)	11/9/2015	

COPYRIGHT AND CONFIDENTIALITY NOTICE

The work described in this document was performed as part of the Go4Hybrid project (Grey Area Mitigation for Hybrid RANS-LES Methods) which is funded by the European Union under Grant Agreement No. 605361.

The project is a collaboration between CFDB, NTS, DLR; FOI, NLR, ONERA, and UniMAN, with Bombardier Transportation, GE Global Research, NUMECA, EDF, PSA Peugeot-Citroen, Rolls-Royce Deutschland, SAAB, ANSYS and Volkswagen AG as observers.

EADS CASSIDIAN and Eurocopter Deutschland GmbH are associate partners, not belonging to the consortium directly.

The opinions, findings and conclusions expressed in this report are those of all partners, and do not necessarily reflect those of the European Commission.

No part of this publication may be reproduced or transmitted in any form
or by any means, whether electronic, mechanical, photocopying or
recording or otherwise; nor stored in any information retrieval system of any kind;
nor used for tendering or manufacturing; nor communicated to any person,
without the prior written permission of the Go4Hybrid consortium
represented by the Project Partners.

The contents of this document must be treated as confidential and protected as
defined in the terms and conditions of the Go4Hybrid Collaboration Agreement (CA).

Table of Contents **Page**

1 Introduction

In task 2.2, the most promising non-zonal methods for Grey Area Mitigation (GAM) developed in task 2.1 are applied to a number of complex test cases. This deliverable gives a preliminary description of the performance of these non-zonal GAM methods on complex test cases, based on the results available a half year before the end of the project. The final description, based on all computational results, will be part of the final report of the project.

2 Non-zonal GAM approaches used for complex test cases

The following non-zonal GAM approaches have been used so far by different partners:

- NTS has considered a modification of the turbulence length scale (or filter width) Δ as used in the SA-DDES approach, replacing the traditional length scale $\Delta_{\max}$ with the modified length scale $\Delta_{\mathrm{SLA}} = \widetilde{\Delta}_{\omega} F_{\mathrm{KH}}$, with the length scale $\widetilde{\Delta}_{\omega}$ sensitized to the direction of the vorticity vector and with the Kelvin-Helmholtz sensor F_{KH} detecting quasi 2D regions.
- CFDB has considered the σ algebraic eddy-viscosity model of Nicoud *et al*. as basic SGS model (instead of Smagorinsky) for SA-DDES, denoted as SA-σ-DDES, in combination with the vorticity-sensitized length scale $\widetilde{\Delta}_{\omega}$.
- NLR has considered a High-Pass Filtered (HPF) SGS model in combination with a spatially and temporally correlated stochastic backscatter SGS model, applied to X-LES.
- FOI has considered an energy-backscatter function for HYB0, denoted as HYB0M, in combination with a modified length scale $\Delta_{\min}$.

These GAM approaches are described in detail in deliverable D2.1-06.

3 Status of complex test cases

3.1 Overview

The status of computations with non-zonal GAM approaches for the complex test cases is given in Table 1 (see the DoW and the test case sections on the Go4Hybrid website for the definition of these cases). For each case, at least two partners have planned to perform non-zonal computations. So far, the most results have been obtained for test case I.5 (Round jet).

Table 1 Status of complex test cases for non-zonal methods (N = new result, P = planned/running, R = reference result)

	CFDB	NTS	FOI	NLR	UniMAN
I.1 Helicopter	P R				P
I.2 Delta wing	N			P R	
I.3 3-element airfoil		N	N	P	P
I.4 2D hump		N R	P		
I.5 Round jet	N	N R		N	

3.2 I.1 Helicopter

There are no GAM results available yet for this case. Reference SST-DDES results from a precursor project have been made available by CFDB and computations using standard SA-DDES have been carried out by UniMAN. Furthermore, the observer Exa has contributed results using their PowerFLOW approach. Computations using GAM methods are planned or running by CFDB and UniMAN.

3.3 I.2 Delta wing

This test case consists of the NASA delta wing with sharp leading edge (used in VFE-2):

- flow conditions with vortex breakdown ($\alpha = 23°$, $M_\infty = 0.07$, $Re_{\text{mac}} = 10^6$),
- experiment of TU Munich,
- mandatory structured grid (6.3 million cells).

Further details are given in the test case definition report.

For this case, CFDB has performed computations with SA-σ-DDES together with the $\widetilde{\Delta}_\omega$ length scale as well as with standard SA-DDES (and standard length scale $\Delta_{\max}$) as a baseline reference. NLR has performed delayed X-LES computations with the HPF SGS model as well as standard SST-DDES as a baseline reference (both results from the ATAAC project).

Instantaneous turbulent structures are shown in Figure 1. The baseline results show steady results over the front part of the wing without any resolved turbulence (subfigures a and c). The helical structures seen there are in fact steady flow features. Including the GAM approaches (subfigures b and d), dramatic effects are seen, with fine-scale instabilities already starting close to the apex of the wing. Contrary to the baseline results, the flow then rapidly develops full 3D turbulence.

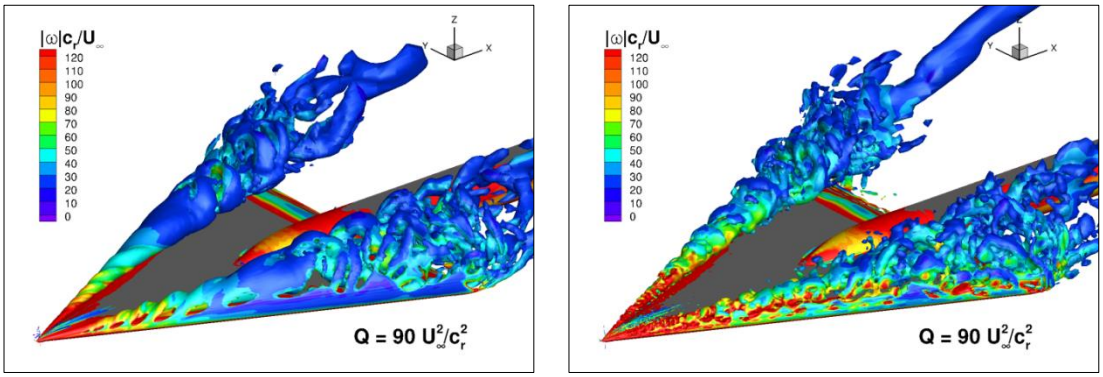

a) SA-DDES + $\Delta_{\max}$ (CFDB) b) SA-σ-DDES + $\widetilde{\Delta}_\omega$ (CFDB)

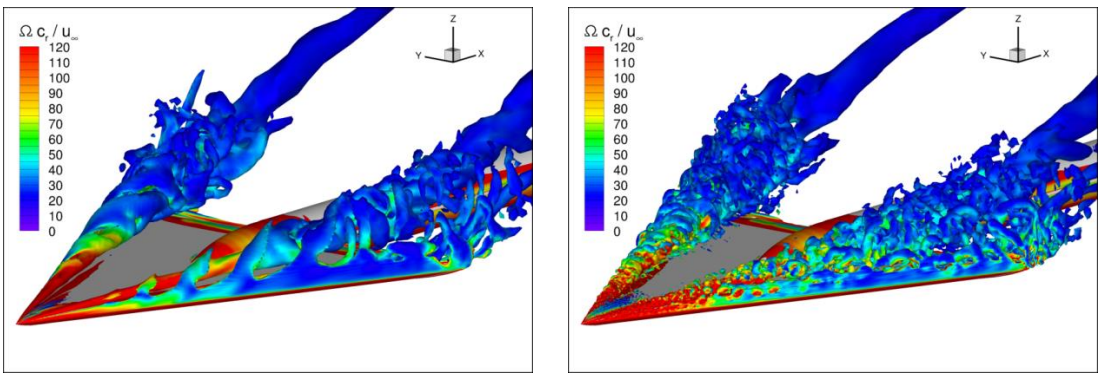

c) SST-DDES (NLR) d) HPF DX-LES (NLR)

Figure 1 Test case I.2 Delta wing: Instantaneous iso-contours of Q-criterion coloured with vorticity magnitude for original methods (left) and methods with GAM approaches (right).

The dramatic impact on the level of resolved turbulence by the GAM approaches is also visible in the level of resolved turbulent kinetic energy as show in Figure 2 at station x/c = 0.4. At this station, there is practically no resolved turbulence in the two baseline computations. Both GAM approaches give a strong and similar improvement, with turbulence levels close to those found in the experiment.

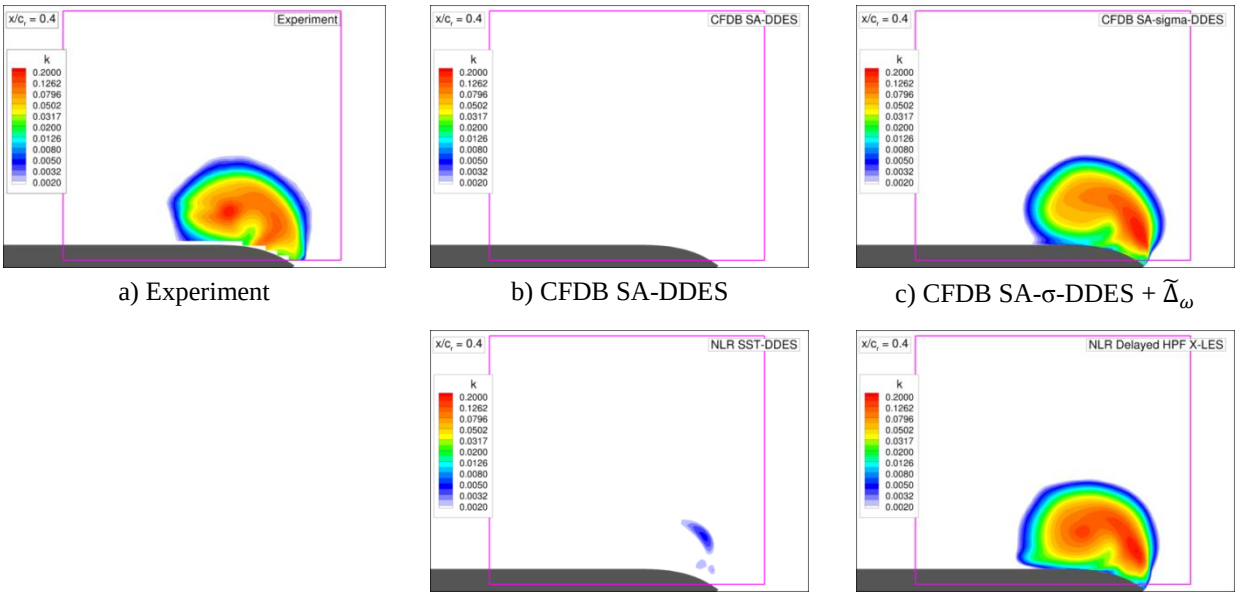

a) Experiment b) CFDB SA-DDES c) CFDB SA-σ-DDES + $\widetilde{\Delta}_{\omega}$

d) NLR SST-DDES d) NLR HPF DX-LES

Figure 2 Test case I.2 Delta wing: Resolved turbulent kinetic energy at station x/c = 0.4.

The mean and RMS values of the pressure coefficient are compared to the experimental results in Figure 3 and Figure 4. At the first two upstream stations (x/c = 0.2 and 0.4), there are hardly any pressure fluctuations present in the baseline results, consistent with the lack of resolved turbulence. As a consequence, in particular the SST-DDES result shows a strong secondary separation at the first station, which is not present in the other computations nor in the experimental result. Further downstream, the baseline results (in particular SA-DDES) tend to show too high levels of pressure fluctuations, indicating too high levels of resolved turbulence, leading to a reduced vortex strength and a reduced suction peak below the vortex (in particular at x/c = 0.6 and 0.8). The two GAM approaches show fairly consistent levels of pressure fluctuations that are also consistent with experiment, in particular at the first three stations. Except for the first station, the suction peak and therefore the vortex strength is close to the experiment. Also the pressure plateau outboard of the suction peak compares well to the experiment, indicating a similar level of secondary separation (which is weak or not present at all).

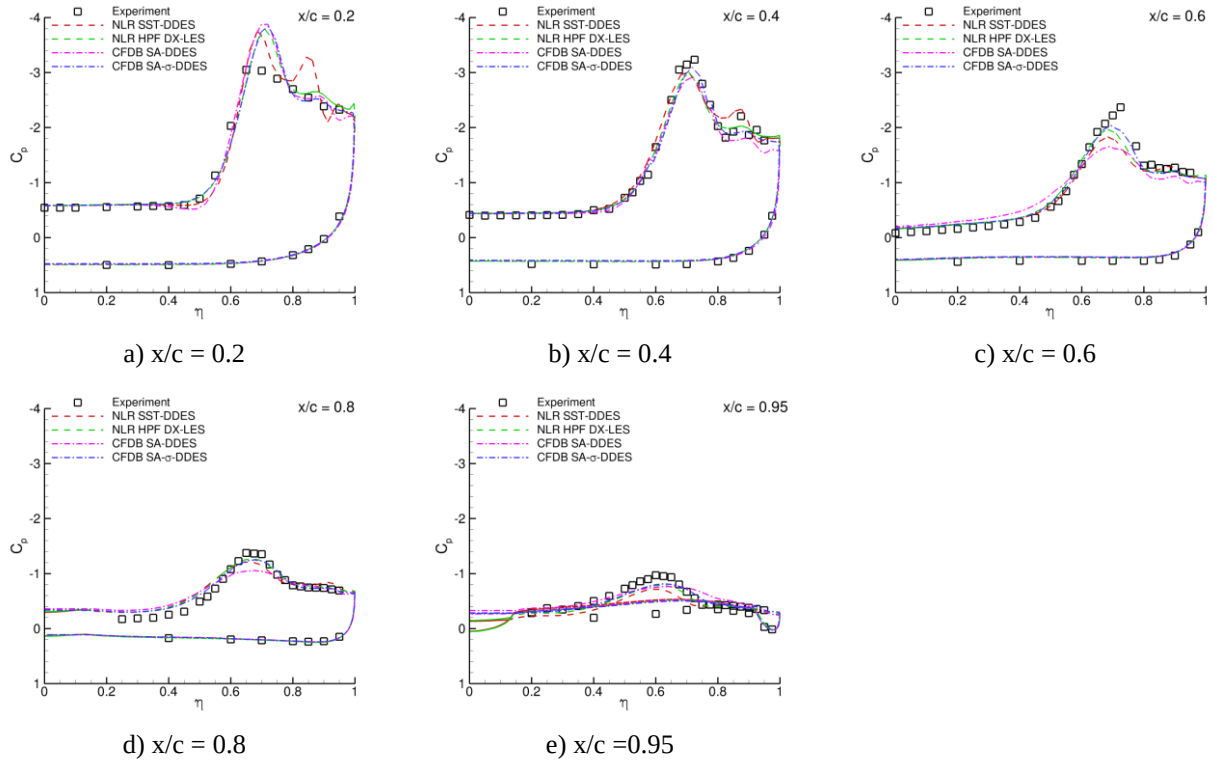

a) x/c = 0.2 b) x/c = 0.4 c) x/c = 0.6

d) x/c = 0.8 e) x/c =0.95

Figure 3 Test case I.2 Delta wing: Mean pressure coefficient at five chord-wise stations.

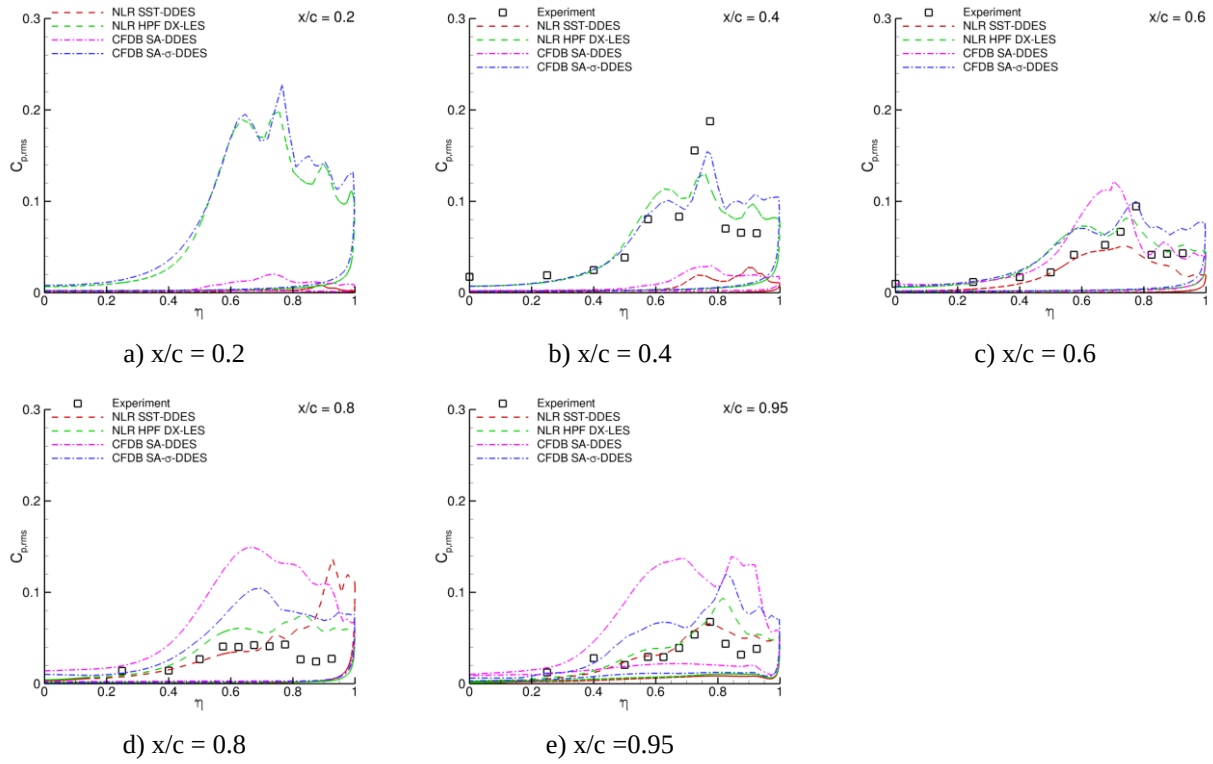

a) x/c = 0.2 b) x/c = 0.4 c) x/c = 0.6

d) x/c = 0.8 e) x/c =0.95

Figure 4 Test case I.2 Delta wing: RMS of pressure coefficient at five chord-wise stations.

3.4 I.3 Three-element airfoil

This test case concerns the F15 three-element airfoil:

- flow conditions: $\alpha = 6°$, $M_\infty = 0.15$, $Re_c = 2.094 \cdot 10^6$,
- experiment of DLR in LEISA project,
- mandatory structured grid (270,000 points in 2D plane, span of 8% chord with 100 points).

Further details are given in the test case definition report.

For this case, NTS has performed computations on the mandatory grid using SA-IDDES with the Δ_{SLA} length scale, as well as with the Δ_{max} length scale as baseline result. The use of $\Delta = \Delta_{SLA}$ leads to some acceleration of the Kelvin-Helmholtz instability in shear layers (Figure 5), but does not cause any visible alteration of the mean skin-friction and pressure coefficients (Figure 6).

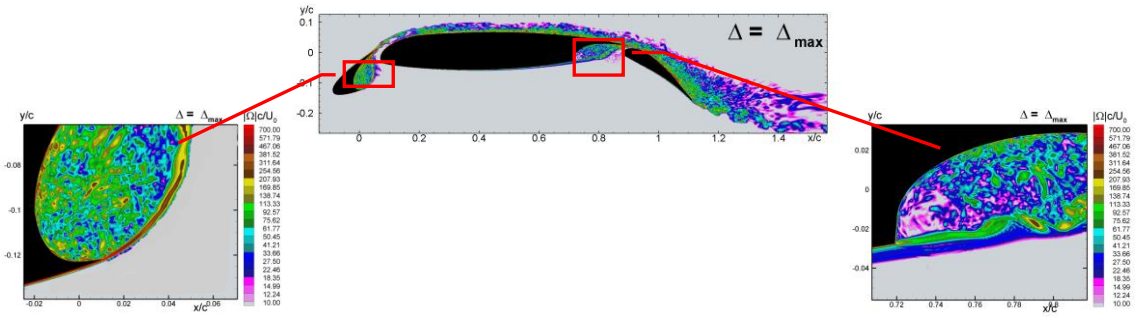

a) SA-IDDES with Δ_{max}

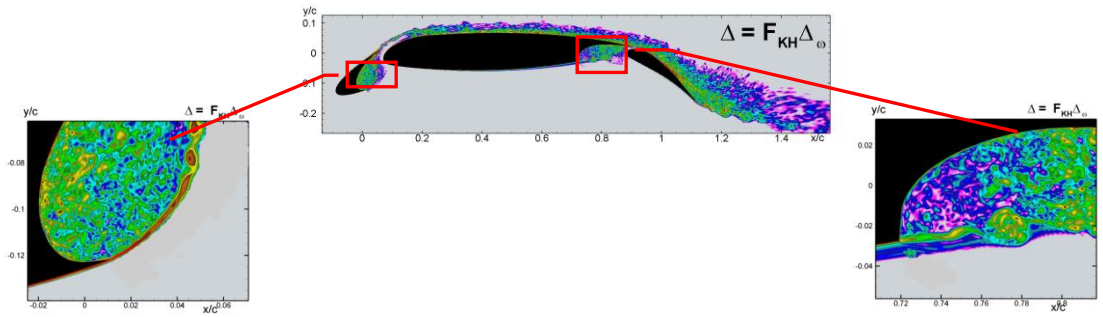

b) SA-IDDES with Δ_{SLA}

Figure 5 Test case I.3 Three-element airfoil: Instantaneous vorticity magnitude for SA-IDDES (NTS) without (a) and with GAM approach (b).

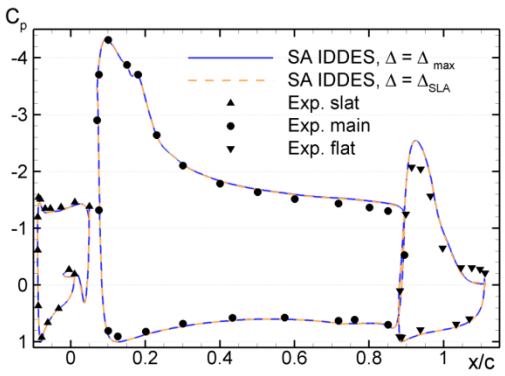

a) Mean pressure coefficient (C_p)

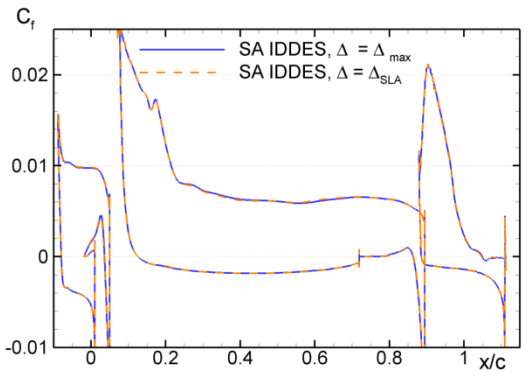

b) Mean skin-friction coefficient (C_f)

Figure 6 Test case I.3 Three-element airfoil: Time-averaged and span-averaged pressure and skin-friction coefficients for SA-IDDES (NTS) without and with GAM approach.

FOI has performed computations on the unstructured grid from the ATAAC project (19,700 points in 2D plane, span of 8% chord with 40 points) using HYB0M with Δ_{min}, as well as computations using HYB0 with Δ_{max} as baseline (from the ATAAC project). From the instantaneous turbulence structures (Figure 7) as well as from the resolved turbulent kinetic energy (Figure 8), it can be seen that HYB0M with Δ_{min} shows relatively high resolved energy in the cove of main wing and a more shallow separation on the aft part of the flap. This has lead to a higher lift of the airfoil, as shown by the mean pressure coefficient (Figure 9). To draw more definitive conclusions, the HYB0M computation needs to be run over more time steps for statistical analysis. Also, the mandatory grid and settings will be used.

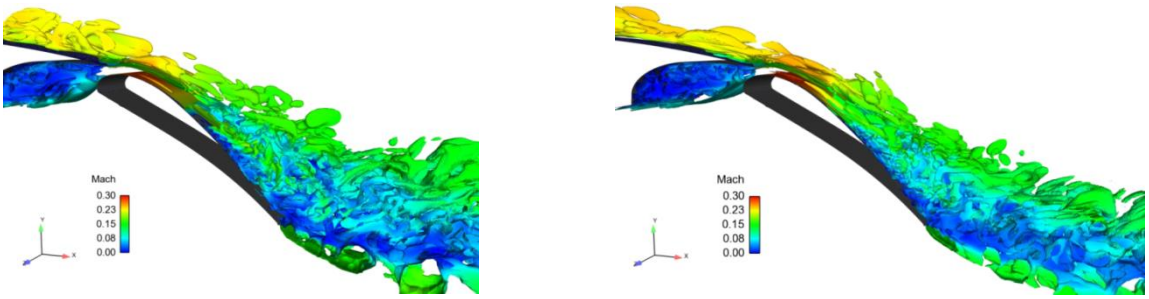

a) HYB0 (FOI) b) HYB0M-min (FOI)

Figure 7 Test case I3 Three-element airfoil: Instantaneous iso-contours of Q-criterion coloured with Mach number for HYB0 (FOI) without (a) and with (b) GAM approach.

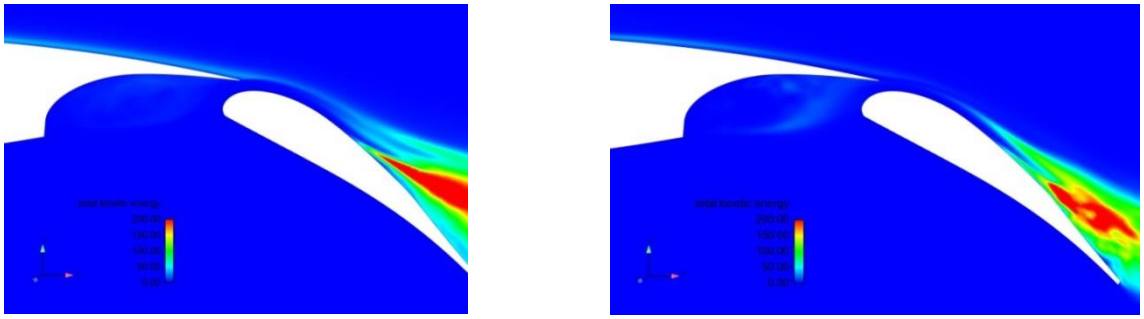

a) HYB0 (FOI) b) HYB0M-min (FOI)

Figure 8 Test case I3 Three-element airfoil: Resolved turbulent kinetic energy for HYB0 (FOI) without (a) and with (b) GAM approach.

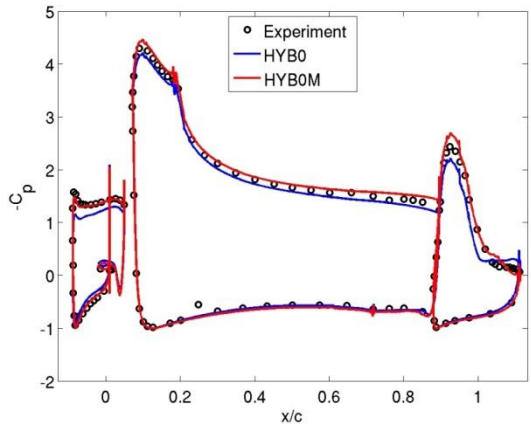

Figure 9 Test case I3 Three-element airfoil: Time-averaged and span-averaged pressure coefficient (C_p) for HYB0 (FOI) without and with GAM approach (HYB0M).

3.5 I.4 2D hump

This case consists of a 2D wall mounted hump:

- flow conditions: $U_\infty = 34.6\ \mathrm{m/s}$, $Re_c = 936{,}000$,
- experiment by Greenblatt *et al*. (2004, 2005),
- mandatory structured grid ($511 \times 127 \times 81$ cells).

Further details are given in the test case definition report.

NTS has performed SA-DDES computations with Δ_{SLA} as well as with Δ_{max} as a baseline. Both computations are in RANS mode up to the separation location and the grey area is therefore located just downstream of separation. NTS has also performed an SA-IDDES computation (with Δ_{max}) as a reference, since it treats the boundary layer upstream of separation already in WM-LES mode, and therefore does not have the grey area downstream of separation.

The use of Δ_{SLA} results in unlocking of the Kelvin-Helmholtz instability and accelerating transition to developed 3D turbulence (Figure 10). As a result, mean pressure and skin-friction prediction tangibly improves and gets close to that of SA-IDDES with Δ_{max} (Figure 11). This improvement is also seen in prediction of the reattachment point (Table 2).

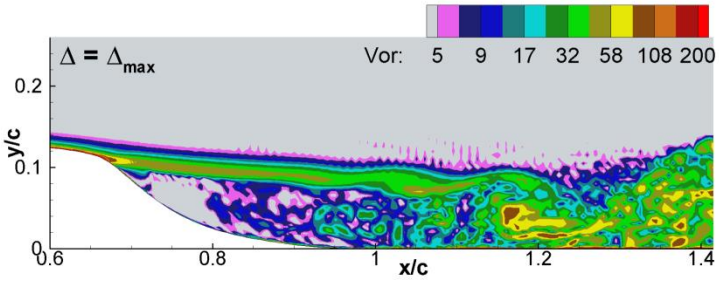

a) SA-DDES with Δ_{max}

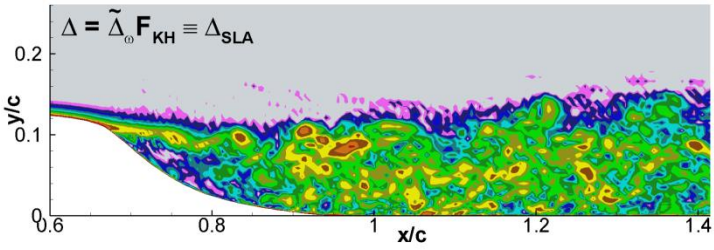

b) SA-DDES with Δ_{SLA}

Figure 10 Test case I.4 2D hump: Instantaneous vorticity magnitude for SA-DDES (NTS) without (a) and with GAM approach (b).

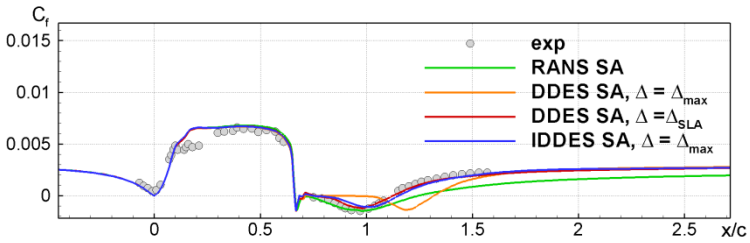

a) Mean skin-friction coefficient C_f

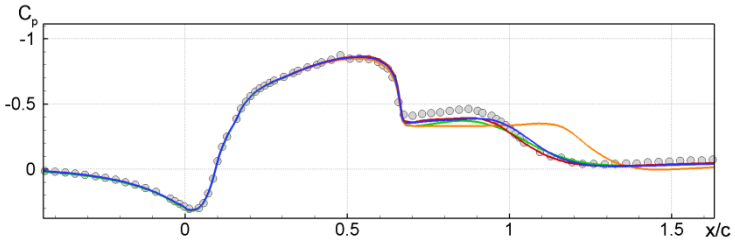

b) Mean pressure coefficient C_p

Figure 11 Test case I.4 2D hump: Time-averaged and span-averaged skin-friction and pressure coefficients for SA-DDES (NTS) without and with GAM approach, compared to SA-RANS and SA-IDDES.

Table 2 Test case I.4 2D hump: Locations of separation and reattachment points for SA-DDES (NTS) without and with GAM approach, compared to SA-RANS and SA-IDDES.

Model	Separation	Reattachment
SA RANS	0.66	1.24
SA DDES, $\Delta = \Delta_{\max}$	0.66	1.32
SA DDES, $\Delta = \Delta_{\mathrm{SLA}}$	0.66	1.13
SA IDDES, $\Delta = \Delta_{\max}$	0.66	1.15
Experiment	0.67	1.12

3.6 I.5 Round jet

This test case consist of an unheated, static round jet:

- $M_\infty = 0.9$ and $Re_D = 1.1 \cdot 10^6$,
- RANS profiles prescribed at nozzle exit plane,
- experimental data: Bridges *et al.*,
- common structured grid "G3" (8.8 million cells).

For this case, CFDB has provided preliminary results for SA-σ-DDES with $\widetilde{\Delta}_\omega$ (covering a relatively short time sample and with some issues with numerics and boundary-condition settings still remaining), NLR has provided results for X-LES with HPF and correlated stochastic backscatter, and NTS for SA-DDES with Δ_{SLA}.

With standard DES methods, there is a pronounced Grey Area, as can be seen in Figure 12a. For all three new results, this Grey Area is significantly reduced (Figure 12b, c, d). As a consequence, the results compare well to experimental results in terms of mean and RMS of velocity (Figure 13, Figure 14, and Figure 15), in particular for the NLR and NTS results, that are also very close to each other. The fact that the CFDB results differ somewhat may be related to the precise set-up of the computation (in particular the nozzle exit boundary condition as well as some other numerical settings); these issues will be tackled by CFDB in their final computations.

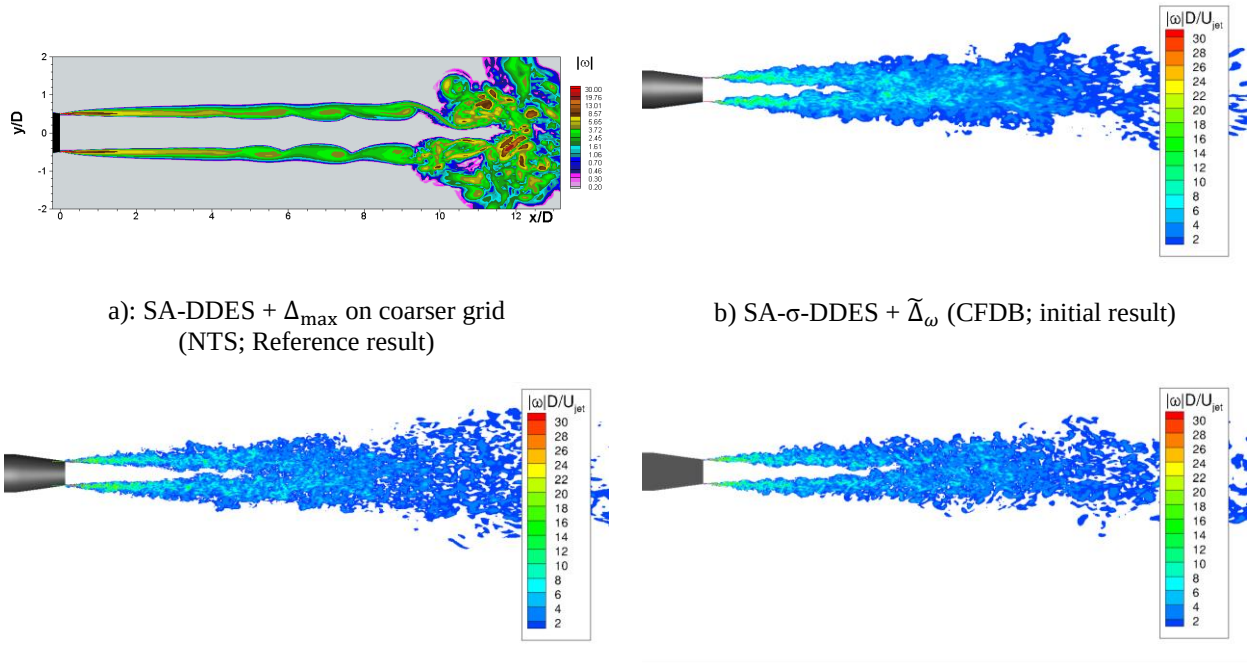

a): SA-DDES + Δ_{max} on coarser grid (NTS; Reference result)

b) SA-σ-DDES + $\widetilde{\Delta}_\omega$ (CFDB; initial result)

c) X-LES + HPF + stochastic backscatter (NLR)

d) SA-DDES + Δ_{SLA} (NTS)

Figure 12 Test case I.5 Round jet: Instantaneous vorticity magnitude

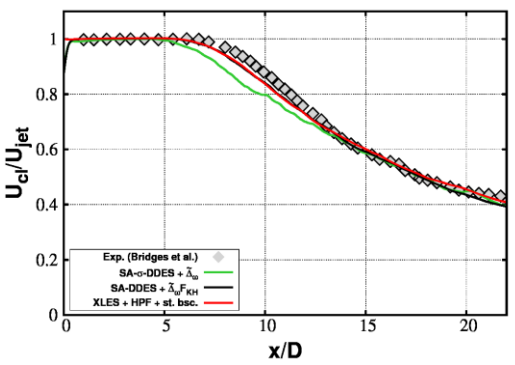

a) Mean velocity along centreline

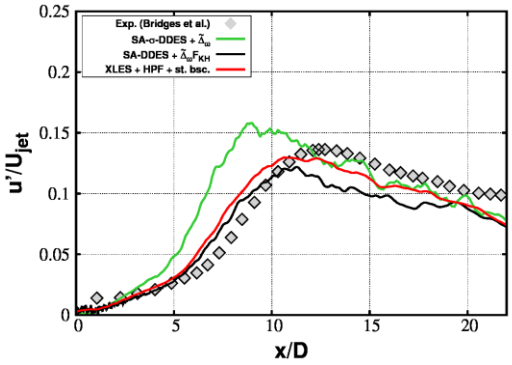

b) RMS velocity along centreline

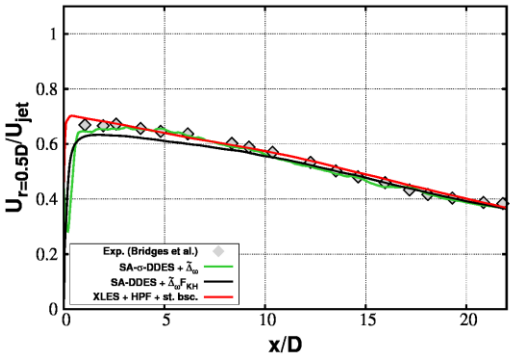

c) Mean velocity along lip line

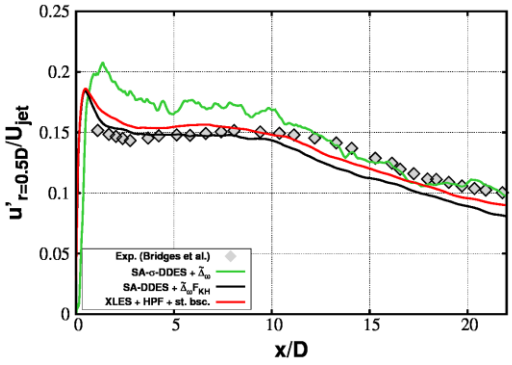

d) RMS velocity along lip line

Figure 13 Test case I.5 Round jet: Mean and RMS velocity (x-component) along jet centreline (r/D = 0) and along lip line (r/D = 0.5).

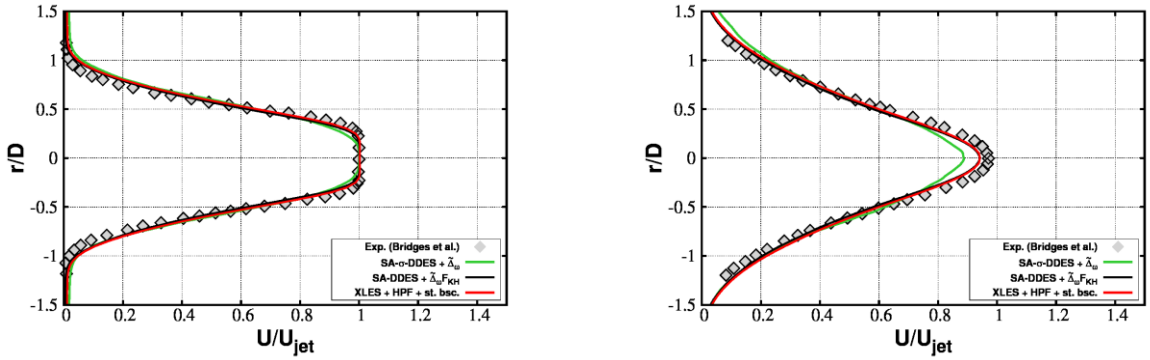

a) x/D = 4.0 b) x/D = 8.0

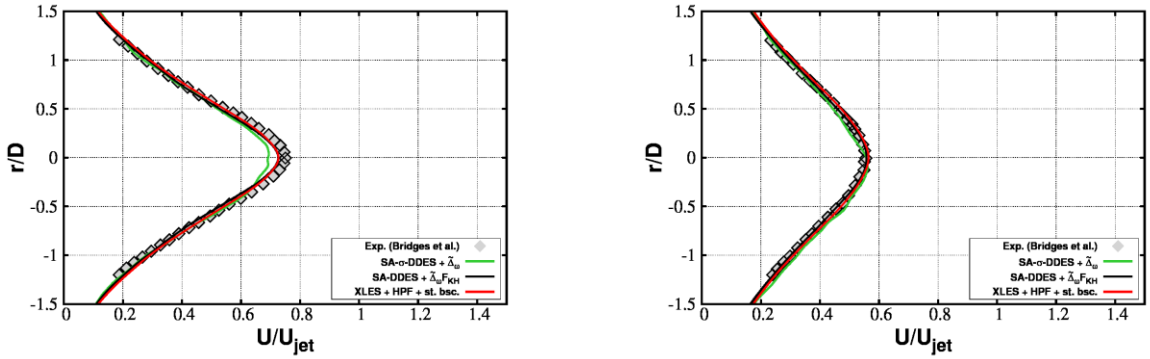

c) x/D = 12.0 d) x/D = 16.0

Figure 14 Test case I.5 Round jet: Mean velocity profiles (x-component) at four cross-stream stations

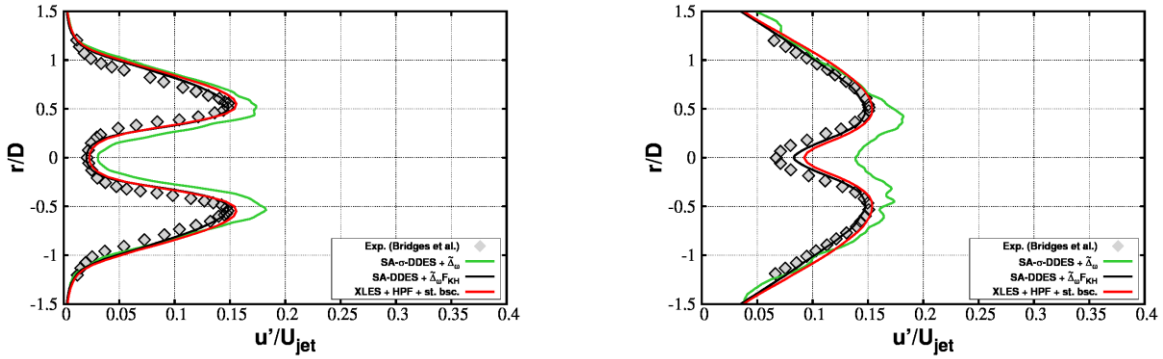

a) x/D = 4.0 b) x/D = 8.0

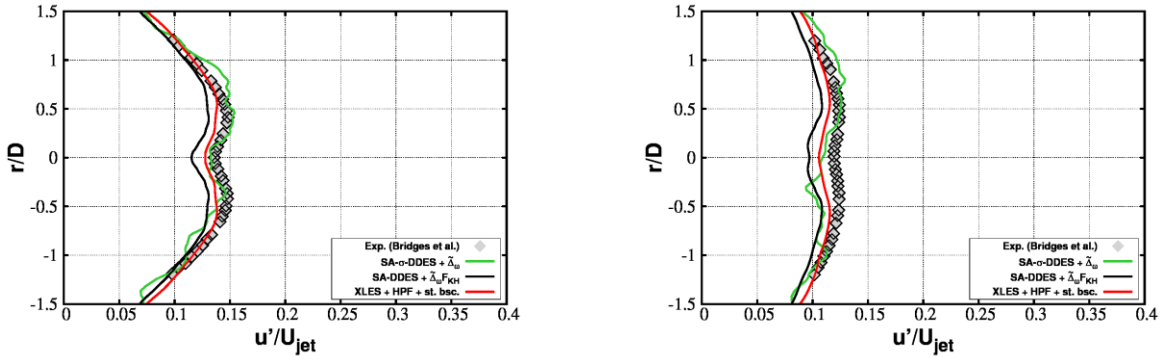

c) x/D = 12.0 d) x/D = 16.0

Figure 15 Test case I.5 Round jet: RMS-velocity profiles (x-component) at four cross-stream stations

4 Conclusions

Based on the computational results for complex test cases available so far, the following preliminary conclusions can be drawn:

- For the delta wing, the 2D hump, and the jet, significant mitigation of the grey area is seen for the three approaches of CFDB (SA-σ-DDES with $\widetilde{\Delta}_{\omega}$), NLR (HPF X-LES with correlated stochastic backscatter), and NTS (SA-DDES with Δ_{SLA}).
- For the delta wing, the GAM methods of CFDB and NLR give very similar results and show strong improvements in terms of levels of pressure fluctuations and resolved turbulence.
- For the 2D hump, the GAM method of NTS shows significant improvement in terms of skin-friction and pressure distribution as well as the location of the reattachment point.
- For the jet, the GAM methods of NTS and NLR give very comparable results with excellent prediction of aerodynamic jet characteristics in terms of mean and RMS of velocity.
- For the 3-element airfoil, the use of Δ_{SLA} is neutral in IDDES, in the sense that it does not lead to any non-desirable side-effects caused by interaction with empirical functions of IDDES.